JACS
JOURNAL OF THE AMERICAN CHEMICAL SOCIETY
Article
pubs.acs.org/JACS

A Versatile Method for the Preparation of Ferroelectric Supramolecular Materials via Radical End-Functionalization of Vinylidene Fluoride Oligomers

Miguel García-Iglesias,[†] Bas F. M. de Waal,[†] Andrey V. Gorbunov,[§] Anja R. A. Palmans,[†] Martijn Kemerink,[§,‡] and E. W. Meijer*[,†]

[†]Institute of Complex Molecular Systems, Laboratory of Macromolecular and Organic Chemistry, Eindhoven University of Technology, P.O. Box 513, 5600 MB Eindhoven, The Netherlands

[§]Department of Applied Physics, Eindhoven University of Technology, P.O. Box 513, 5600 MB Eindhoven, The Netherlands

[‡]Complex Materials and Devices, Department of Physics, Chemistry and Biology (IFM), Linköping University, 58183 Linköping, Sweden

Supporting Information

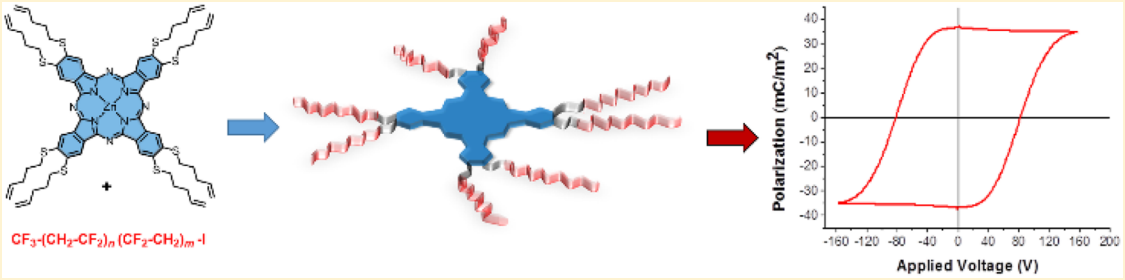

ABSTRACT: A synthetic method for the end-functionalization of vinylidene fluoride oligomers (OVDF) via a radical reaction between terminal olefins and **I-OVDF** is described. The method shows a wide substrate scope and excellent conversions, and permits the preparation of different disc-shaped cores such as benzene-1,3,5-tricarboxamides (BTAs), perylenes bisimide (PBI), and phthalocyanines (Pc) bearing three to eight ferroelectric oligomers at their periphery. The formation, purity, OVDF conformation, and morphology of the final adducts has been assessed by a combination of techniques, such as NMR, size exclusion chromatography, differential scanning calorimetry, polarized optical microscopy, and atomic force microscopy. Finally, **PBI-OVDF** and **Pc-OVDF** materials show ferroelectric hysteresis behavior together with high remnant polarizations, with values as high as $P_r \approx 37$ mC/m^2 for **Pc-OVDF**. This work demonstrates the potential of preparing a new set of ferroelectric materials simply by attaching OVDF oligomers to different small molecules. The use of carefully chosen small molecules paves the way to new functional materials in which ferroelectricity and electrical conductivity or light-harvesting properties coexist in a single compound.

INTRODUCTION

Ferroelectric and piezoelectric materials play a vital role in modern technologies ranging from capacitors, hydrophones, and actuators to frequency-controlled devices.[1] To further advance these technologies, access to cheaper and readily processable materials that show large ferroelectric and piezoelectric responses is highly desired. Organic materials are currently explored, as they are potentially cheap, easily processable, and biocompatible, and they can be endowed with diverse and tunable functions. In addition, their mechanical flexibility is crucial for piezoelectric applications.

Since the discovery of the first organic ferroelectric material in 1920,[2] the observation of ferroelectric properties in organic materials has not been profuse.[3] In fact, most of the organic ferroelectric research is focused on poly(vinylidene fluoride) (PVDF).[4] PVDF displays a large remnant polarization, a short switching time, and an excellent thermal stability, which make it suitable for the fabrication of piezoelectric films.[5] The ferro- and piezoelectric properties of PVDF originate from the antiparallel intrachain arrangement of alternating CH_2 and CF_2 segments in a zigzag all-*anti* conformation—the so-called *β*-form.[6] However, untreated PVDF thin films processed from the melt or from solution are not ferroelectric.[6b] They possess a mixture of *α*, *β*, and *γ* conformations,[4] and additional steps, such as mechanical stretching,[5b] thermal annealing,[7] and electrical poling,[8] have to be performed in order to achieve the *β*-phase necessary for them to display ferro- and piezoelectric properties.

More recently, vinylidene fluoride oligomers (OVDF) and poly(vinylidene fluoride−trifluoroethylene (P(VDF-*co*-TrFE), a copolymer based on PVDF) have been evaluated to enhance

Received: February 20, 2016
Published: April 27, 2016

DOI: 10.1021/jacs.6b01908
J. Am. Chem. Soc. 2016, 138, 6217−6223

Scheme 1. Structure of the Discotic Molecules BTA-OVDF, PBI-OVDF, and Pc-OVDF

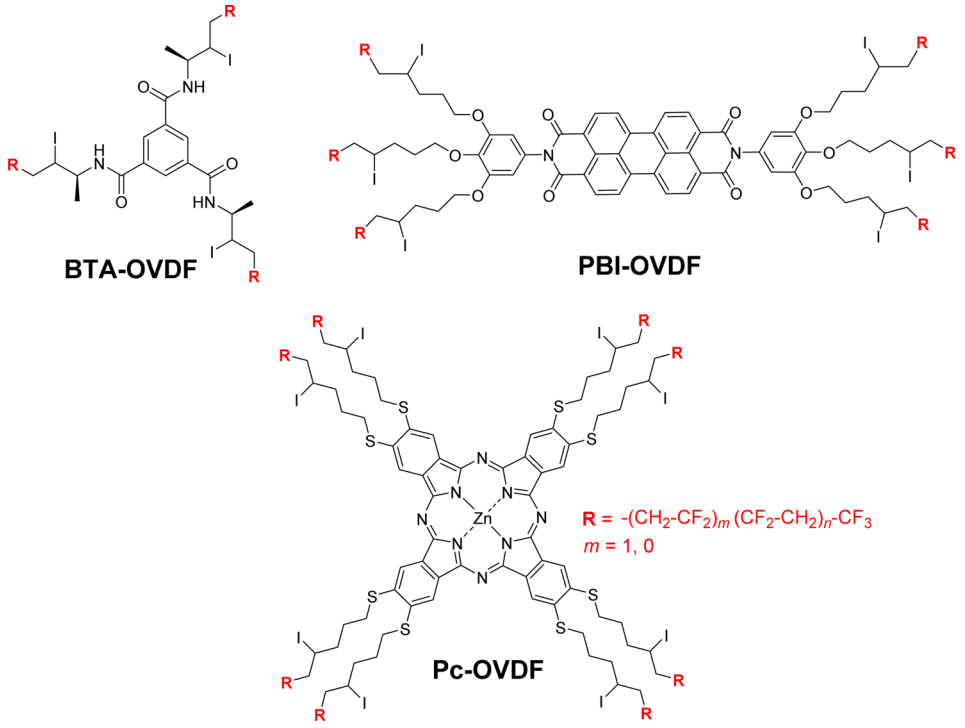

the formation of the β-phase. In OVDFs with a degree of polymerization smaller than 10, the ferroelectric β-form is spontaneously formed when the film is processed from a solution of polar solvents.[9]

In contrast to polymers, OVDFs can be readily vapor deposited without decomposition of the material.[10] In addition, their ferroelectric properties are better than those reported for the polymers.[11] Also in P(VDF-*co*-TrFE), the β-form arises spontaneously from solution. The presence of the PTrFE block induces an all-*trans* stereochemical conformation due to steric hindrance from the additional fluorine atoms.[6a,12]

Because of the interesting properties of OVDF, inclusion complexes of OVDF with zeolites and cyclodextrins have been studied.[13] However, to date, the covalent coupling of OVDF with organic molecules has not been reported. Attaching oligomers of VDF covalently to small and well-defined molecules opens up many possibilities to induce ferroelectric and piezoelectric properties in different materials. In addition, the beneficial OVDF processing properties could be synthetically tuned with careful design of the small molecules. Moreover, the combination of ferroelectric properties with other properties, such as semiconducting or light-harvesting properties, by blending the different components becomes accessible, which would represent a significant advantage in the field of nonvolatile memory devices[14] and solar cells.[15] Recent progress combining semiconducting core molecules substituted at the periphery with appropriately flexible alkyl chains has resulted in unprecedented physical properties due to the rational design of the side chains which control the packing of the columnar aggregates and therefore the charge-carrier mobilities along them.[16] Thus, the union of small light-harvesting or semiconducting molecules with covalently attached OVDF could give rise to materials with improved optoelectronic properties due to the higher interfacial area and the absence of phase separation issues that are inherent to conventional blended systems, where ferroelectric and semiconducting functionalities are introduced by different compounds.

Herein, we show the synthesis and characterization of OVDF covalently coupled to a variety of organic scaffolds—scaffolds that can order themselves into supramolecular morphologies. In order to achieve this, a radical addition of $CF_3(CH_2CF_2)_n(CF_2CH_2)_mI$ (m = 0, 1 and $n \approx 6$), **I-OVDF**, to terminal olefins is introduced. This radical reaction allows the synthesis of three different central cores bearing three to eight OVDF oligomers at their periphery (Scheme 1). The central cores were selected to fulfill different aims. Benzene-1,3,5-tricarboxamides (BTAs) are known to exhibit ferroelectric properties due to the possibility to orient the amides forming a macrodipole.[17] On the other hand, perylene bisimides (PBI) and phthalocyanines (Pc) were selected because they display high extinction coefficients[18] and semiconducting properties.[19] These characteristics, in combination with the ferroelectric properties arising from the OVDF side chains, can be used in the fabrication of future optoelectronic devices. A full characterization of the bulk and ferroelectric properties of these novel materials is presented.

RESULTS AND DISCUSSION

Synthesis and Characterization. In order to circumvent the troublesome synthesis of the vinylidene fluoride oligomers, we selected $CF_3(CH_2CF_2)_n(CF_2CH_2)_mI$ (m = 0, 1 and $n \approx 6$) (**I-OVDF**),[18b] kindly provided by DAIKIN, and developed a method to couple these OVDF precursors to the scaffold selected (Scheme 1). The ^{1}H NMR spectrum of **I-OVDF** in deuterated acetone showed two signals centered at 3.61 and 3.86 ppm, with a ratio of the signal intensities of 3:1. Those peaks were assigned to methylene protons of the terminal VDF unit carrying an iodine atom as end group attached to $-CH_2CF_2I$ or to $-CF_2CH_2I$, respectively. In addition, the ^{19}F NMR spectrum of **I-OVDF** showed a peak at −38 ppm,

DOI: 10.1021/jacs.6b01908
J. Am. Chem. Soc. 2016, 138, 6217−6223

Scheme 2. Synthetic Method for the End-Functionalization of Oligo(vinylidene fluoride)

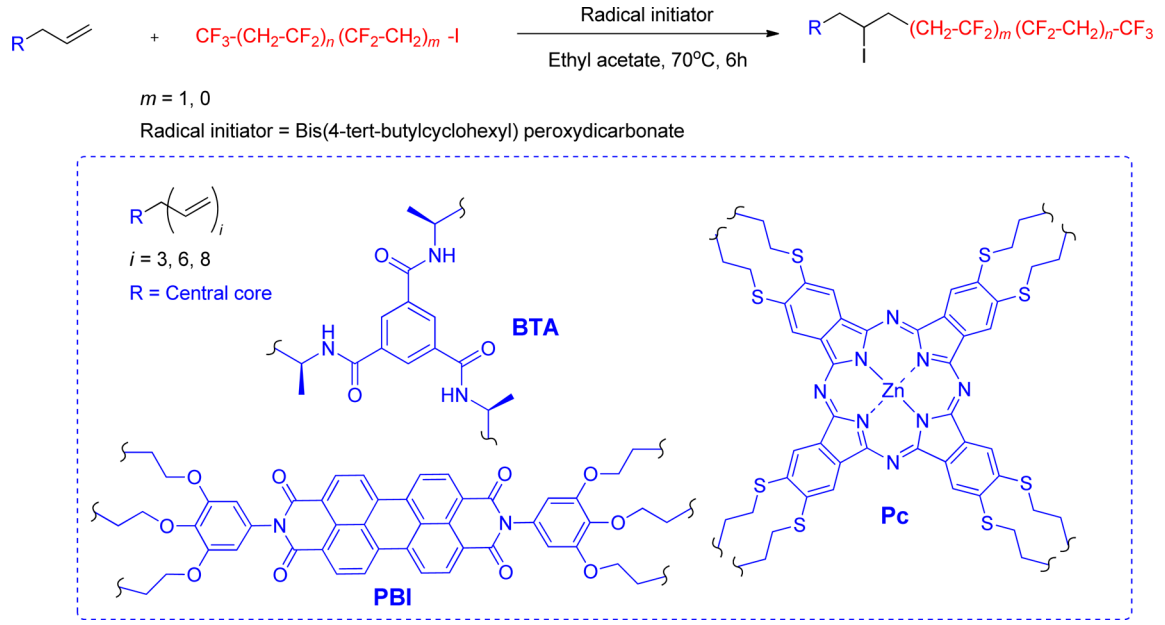

corresponding to $-CH_2\underline{CF_2}I$, and peaks at −110 and −115 ppm, corresponding to $-\underline{CF_2}CH_2I$ (see Figures S14 and S15). Hence, **I-OVDF** is a mixture of oligomers, in which the iodine is coupled to either a CH_2 or a CF_2 group.

A number of synthetic coupling strategies were evaluated. The nucleophilic substitution of the iodide for azides, previously described in the literature,[20] was successful and proved to be specific for those oligomers with the iodine coupled to CF_2 groups. However, the subsequent 1−3 dipolar addition of the azido-OVDF to alkynes failed. Alternatively, the procedure developed by Kitagawa[21] to obtain terminal olefins from **I-OVDF** failed in the absence of zeolites. Other reactions, such as fluoroalkylations of arylboronic acids with fluoroalkyl iodides, were tested[22] but only afforded undesired products.

After a full year of trying to use standard organic coupling strategies with a large variety of catalysts, we turned our attention to radical reactions. Radical iodine-transfer polymerizations have been successfully used for the synthesis of **I-OVDF** and copolymers of PVDF.[23] Therefore, we proceeded to couple **I-OVDF** to terminal olefins via a radical reaction. For this purpose, different radical initiators were tested using **BTA** as a model substrate. Applying bis(4-(*tert*-butyl)cyclohexyl) peroxydicarbonate as the radical source and ethyl acetate as the solvent afforded the desired product, whereas other radical initiators did not result in coupling products (Scheme 2). This radical coupling proceeded in mild conditions; heating the mixture at 70 °C for 6 h sufficed to get full conversion.

After the optimal conditions for the coupling reactions were established, **I-OVDF** was reacted with three desired central cores, **BTA**, **PBI**, and **Pc**, substituted with three, six, and eight terminal olefins, respectively. In all cases, inspection of the ^{1}H and ^{19}F NMR spectra of the crude samples showed that the peaks corresponding to CH_2CF_2I and CF_2CH_2I disappeared after 6 h of radical addition. Moreover, the ^{1}H NMR spectra of the crudes also lacked the peaks corresponding to the terminal olefins, indicating their quantitative conversion. After purification by size exclusion chromatography (SEC), **BTA-OVDF**, **PBI-OVDF**, and **Pc-OVDF** were obtained and fully characterized by ^{1}H NMR, ^{19}F NMR, SEC, matrix-assisted laser desorption/ionization time-of-flight mass spectrometry (MALDI-TOF-MS), and UV spectroscopy.

The ^{1}H NMR spectrum of purified **BTA-OVDF** showed Ar−H and N−H resonances at different positions, indicating a loss of symmetry due to the presence of differently terminated chains coupled to the aromatic core. Additionally, the spectra also showed different peaks between 5.2 and 4.5 ppm, corresponding to the protons next to the iodide (see Figure S17). The ^{1}H NMR spectra of **PBI-OVDF** and **Pc-OVDF** showed broader signals, indicative of a high degree of aggregation, which is most likely caused by interactions between aromatic cores (see Figures S20 and S24).

SEC traces measured in THF of both the starting material **I-OVDF** and the final products confirmed the NMR findings. The starting material showed a number-averaged molecular weight (M_n) of 522 g/mol, in line with that expected for $CF_3(CH_2CF_2)_nI$ ($n \approx 6$), and a molar-mass dispersity ($Đ$) of 1.37. The SEC traces of the final products **BTA-OVDF** and **PBI-OVDF** showed significantly lower retention times, indicating higher molecular weights, and no peak at the retention time corresponding to **I-OVDF**. The values for M_n are all in the expected range, between 2.4 and 7.5 kDa for 3−8 times substituted cores, and the molar-mass dispersities are even lower than the dispersity shown by the starting oligomer mixture (see Figure 1 and Table 1).

Whereas SEC and NMR confirmed the attachment of the OVDF chains to the different scaffolds, it remained unclear if the iodine was still present after workup. Thus, all final products were analyzed by MALDI-TOF-MS. **BTA-OVDF** showed a relatively broad molecular weight distribution corresponding to the molecular weight distribution expected for the final compound due to the use of an oligomer mixture ($Đ$ = 1.37). Next to the $[M]^+$ peaks within the spectrum, a second distribution was observed corresponding to $[M - NH_4]^+$ peaks (see Figure 2). Analysis of the masses showed that the molecular weights observed for **BTA-OVDF** correspond with the final molecule bearing three iodine atoms.

The MALDI-TOF spectra of **PBI-OVDF** and **Pc-OVDF** showed broader and less defined distributions, caused by the

DOI: 10.1021/jacs.6b01908
J. Am. Chem. Soc. 2016, 138, 6217−6223

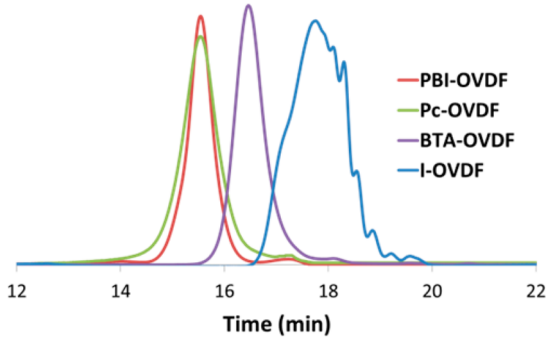

Figure 1. Size-exclusion chromatogram equipped with a PDA detector for **I-OVDF**, **BTA-OVDF**, **PBI-OVDF**, and **Pc-OVDF** using THF as eluent.

Table 1. Molecular Weight and Dispersity for I-OVDF, BTA-OVDF, PBI-OVDF, and Pc-OVDF Determined by GPC Using THF as Eluent[a]

product	M_n [g/mol]	M_w [g/mol]	$Đ$ [-]
I-OVDF	522	718	1.37
BTA-OVDF	2412	2876	1.19
PBI-OVDF	6525	7097	1.09
Pc-OVDF	7557	9253	1.18

[a]SEC calibrated with narrow dispersity polystyrene standards.

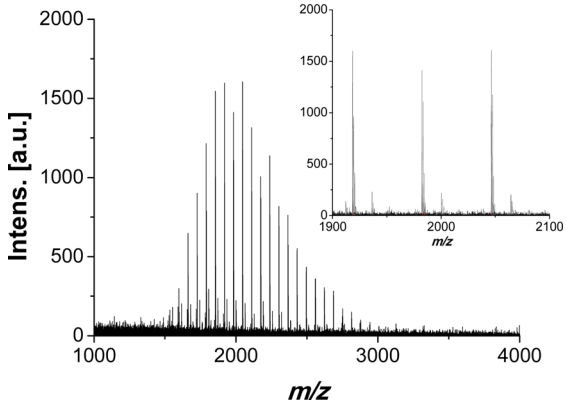

Figure 2. MALDI-TOF-MS spectrum of **BTA-OVDF**.

higher number of OVDF chains located at the periphery of the molecules. However, the molecular weight distribution in both cases was consistent with the results found by SEC (see Figures S22 and S26).

Finally, the characteristic absorption of the PBI and Pc chromophores, located around 485 and 520 nm, and 470 and 700 nm, respectively, were observed by UV spectroscopy for the final compounds **PBI-OVDF** and **Pc-OVDF**. Both compounds showed hypsochromic shifts relative to their precursors, indicative of the formation of H-aggregates in THF. Additionally, compounds **PBI-OVDF** and **Pc-OVDF** showed a strong absorbance at shorter wavelengths due to the presence of the OVDF tails, which confirmed the covalent attachment of the OVDF side chains. (see Figures S28 and S29). In summary, by a combination of different analytical techniques, we demonstrate that the radical coupling between terminal olefins and **I-OVDF** is an effective synthetic tool and results in three new star-shaped molecules that are designed to have morphologies for potential ferroelectric properties.

Thermal Behavior, OVDF Conformation, and Morphology of the Materials. The thermal behavior and the different conformations of the OVDF starting material and the final products were evaluated by differential scanning calorimetry (DSC), polarized optical microscopy (POM), and infrared (IR) spectroscopy. Moreover, the morphology of the drop-casted materials has been studied by atomic force microscopy (AFM).

The starting material **I-OVDF** showed a melting peak around 120 °C with a shoulder at 102 °C, probably the result of lower molecular weight fractions.[9] During cooling, a crystallization peak appeared at 74 °C. The **BTA-OVDF**, **PBI-OVDF**, and **Pc-OVDF** DSC traces did not show shoulders in the melting peaks. They all showed transitions at higher temperatures in the heating and cooling runs compared to **I-OVDF**, although there is not a clear trend upon increasing the number of OVDF chains per molecule (see Table 2 and Figures S16, S19, S23, and S27).

Table 2. Transition Temperatures and Corresponding Enthalpies of I-OVDF, BTA-OVDF, PBI-OVDF, and Pc-OVDF Obtained by DSC Measurements[a]

product	T_1[b] [°C]	ΔH_1 [J/g]	T_2[c] [°C]	ΔH_2 [J/g]
I-OVDF	102.0	5	74.5	37
	122.2	23		
BTA-OVDF	124.2	27	92.7	35
PBI-OVDF	126.4	18	112	20
Pc-OVDF	129	25	110	26

[a]All the DSC data were collected during the second heating and cooling run. [b]T_1 is the transition temperature measured during heating. [c]T_2 is the transition temperature measured during cooling. The cooling and heating rate was 2 K min^{-1}.

The thermal behavior of **I-OVDF**, **BTA-OVDF**, **PBI-OVDF**, and **Pc-OVDF** was further investigated using POM. Under crossed polarizers, **I-OVDF**, **BTA-OVDF**, and **PBI-OVDF** showed birefringent textures after slow cooling from the isotropic melt at a rate of 2 °C/min. Slow cooling induced the growth of a pseudo-focal conic texture, typical for a columnar mesophase, for **BTA-OVDF** and **PBI-OVDF**, indicating long-range order, while **I-OVDF** showed a less ordered texture (see Figure S30). **Pc-OVDF** did not show any birefringence under crossed polarizers upon cooling, indicating the formation of an amorphous material.

IR spectroscopy is a sensitive technique to assess the presence of the different conformations of PVDF in the solid state. PVDF films show strong absorption bands at 1290, 1190, 880, and 840 cm^{-1} when the ferroelectric β-phase is present.[6,24] **I-OVDF**, **BTA-OVDF**, **PBI-OVDF**, and **Pc-OVDF** were analyzed by IR in order to elucidate the conformation of the OVDF within the materials. Drop-casted samples from a THF solution of **I-OVDF** and **BTA-OVDF** showed the characteristic vibrations of the all-*trans* conformation (1270, 1190, 880, and 840 cm^{-1}) at room temperature. When cooling slowly from the isotropic melt, **I-OVDF** retains mostly the β-conformation together with the γ-conformation (1230 cm^{-1}). In contrast, **BTA-OVDF** evolves to the non-ferroelectric α form (1403, 1204, 1183, 975, 874, 794, 760, and 614 cm^{-1}) (see Figure S32). However, the formation of the (presumably aligned) β-form could be achieved by slow cooling in the presence of an electrical field (80 V/μm, Figure 3). For this purpose, we used commercial glass liquid crystal cells with a constant cell spacing

DOI: 10.1021/jacs.6b01908
J. Am. Chem. Soc. 2016, 138, 6217−6223

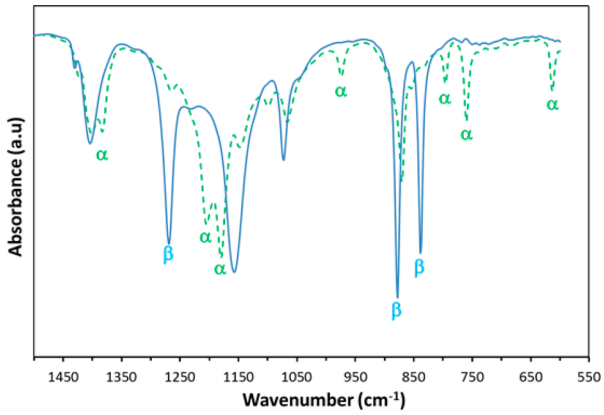

Figure 3. IR spectra of **BTA-OVDF** before (dashed line) and after (solid line) applying an electrical field of 80 V/μm in a liquid crystal cell.

of 5 μm between indium tin oxide (ITO) transparent electrodes. Changes in the morphology of the **BTA-OVDF** liquid crystal were observed by POM by comparing the regions in which the electric field was applied with regions in which it was not (see Figure S31). Such changes are presumably derived from the evolution from the non-ferroelectric α form to the β-conformation and the alignment of the last one when applying an electrical field, which is in good agreement with the IR experiments.

The conformation of **PBI-OVDF** and **Pc-OVDF** side chains was also analyzed by IR. In both cases, the presence of the π-extended cores gave rise to a more amorphous conformation of the OVDF chains, revealing overlapping of the OVDF peaks with the core-derived peaks, as concluded from the comparison of individual IR spectra. A small increase of the β-form was observed when cooling slowly from the isotropic melt, obtaining the highest β-conformation ratio for **PBI-OVDF** and **Pc-OVDF** when applying an electrical field (80 V/μm) while heating the materials to 90 °C (see Figures S33 and S34). X-ray diffraction experiments were carried out on unpoled samples, given the difficulties in analyzing the samples after poling them between gold electrodes to achieve the highest ordered morphology. However, undefined morphologies of the compounds **Pc-OVDF** and **Pc-PDI** were achieved (see Figure S35). The conformation of the OVDF was observed for **BTA-OVDF**, changing from α to β after application of an electrical field of 1 kV for 2 h using a corona poling device (see Figure S36).

Finally, morphological studies of the drop-casted materials were performed by AFM (Figure 4). **BTA-OVDF** showed a very rough surface topology consisting of large domains. In contrast, **PBI-OVDF** and **Pc-OVDF** films displayed completely different morphologies. Both materials produced rather smooth films, on top of which domain-like structures with sizes in the range of hundreds of nanometers can be observed. These domains are probably due to the formation of aggregates by $\pi-\pi$ stacking of the aromatic perylene and phthalocyanine cores in the presence of the OVDF matrix,[25] and to their low solubility at relatively high concentrations.[26] Due to the extreme roughness and the sticky nature of the **BTA-OVDF** material, it was technically not feasible to reliably scan areas larger than a few hundred nanometers. However, even on small areas, we observed a very high surface roughness in comparison to the other materials. In summary, the morphology of the

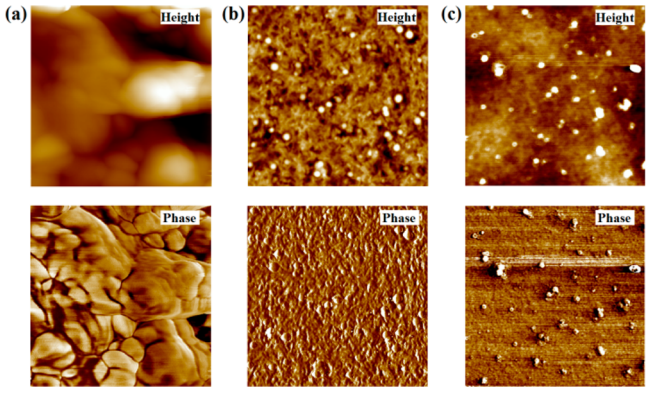

Figure 4. Atomic force microscopy topographical images (height and phase) of drop-cast samples (20 mg/mL in $CHCl_3$) on a glass substrate after annealing at 70 °C for complete solvent evaporation: (a) **BTA-OVDF** (0.385 × 0.385 μm^2), total vertical scales −150 nm and 47° phase degrees; (b) **PBI-OVDF** (5 × 5 μm^2), total vertical scales −50 nm and 44° phase degrees; and (c) **Pc-OVDF** (5 × 5 μm^2), total vertical scales −25 nm and 10° phase degrees.

materials and the conformation of the OVDF of **BTA-OVDF**, **PBI-OVDF** and **Pc-OVDF** within the materials have been analyzed by different techniques. The formation of the highest fraction of β-conformation was observed after applying an electrical field at elevated temperatures, followed by slow cooling. Moreover, **PBI-OVDF** and **Pc-OVDF** showed a tendency to form aggregates in the solid state, which is in agreement with the ^{1}H NMR and UV spectroscopy data obtained in solution as described above.

Electrical Switching Properties. The ferroelectric switching properties of our systems were assessed on metal−ferroelectric−metal (M-F-M) capacitor structures using gold electrodes on a glass substrate. The functional organic films were prepared by drop-casting from a chloroform solution. The active layer thickness ranged from 1 to 4 μm. All materials were first heated while an external electric field was applied (25 V/μm). Slow modulation of the electric field was found to improve the uniform alignment of the macro-dipoles perpendicular to the gold electrodes.[27]

The actual ferroelectric switching experiments were performed on pre-aligned devices. Polarization vs applied field ($P-E$) hysteresis loops were obtained by the double-wave method (DWM, see SI),[28] which makes it possible to suppress the effects of (non-hysteretic) conduction currents from the (hysteretic) displacement current. The latter is integrated vs applied field to obtain the quasi-static polarization shown in Figure 5.

Despite showing the highest degree of ferroelectric β-conformation of all materials investigated here, **BTA-OVDF** showed only paraelectric properties (Figure 5a). The absence of ferroelectric switching may be related to steric hindrance in the densely packed aggregates of **BTA-OVDF** or to the rough morphology that may suppress effective switching.[29] This lack of ferroelectric behavior is more surprising, since both a BTA with alkyl side chains and the **I-ODVF** itself show ferroelectricity, but the combination of them gives a highly dielectric material.

Ferroelectric hysteresis behavior has been found for **PBI-OVDF** and **Pc-OVDF** devices, which showed concave $P-E$ curves, indicative of polar switching (Figures 5b,c). The coercive field (E_C) and remnant polarization (P_r) for saturated polarization of **PBI-OVDF** and **Pc-OVDF** were obtained from

DOI: 10.1021/jacs.6b01908
J. Am. Chem. Soc. 2016, 138, 6217−6223

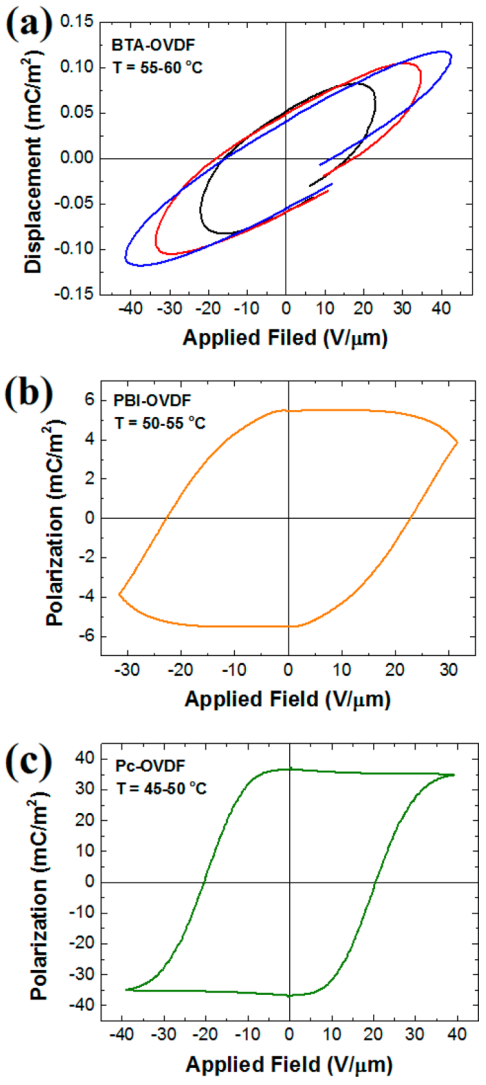

Figure 5. Electrical switching behavior in of OVDF-based supramolecular systems: (a) Typical series of displacement vs field ($D-E$) loops obtained on **BTA-OVDF** at 50−60 °C. Saturated ferroelectric polarization vs field ($P-E$) loops obtained at f = 1 Hz on (b) **PBI-OVDF** at 50−55 °C and (c) **Pc-OVDF** at 45−50 °C.

the quasi-static ferroelectric hysteresis behavior at 50−55 °C.[30] **PBI-OVDF** displayed $E_C \approx 23$ V/μm and $P_r \approx 4$ mC/m^2, which are respectable values for a supramolecular organic ferroelectric.[3d] Nevertheless, the hysteresis loops show convex regions, typical for a lossy dielectric and composite ferroelectric materials exhibiting conductance.[31] This current leakage is likely to result from Ohmic conduction through the semiconducting perylene cores. At the same time, the low crystallinity of the polar units might affect the shape of the hysteresis loop.[32] In addition, slowly responding ionic species can contribute to the non-ideal shape of the $P-E$ curves. Finally, **Pc-OVDF**-based devices show nearly ideal hysteresis behavior, exhibiting a remarkably high remnant polarization ($P_r \approx 37$ mC/m^2) at a similar coercive field ($E_C \approx 20.5$ V/μm). For comparison, properly treated pure OVDF films give $P_r \approx 90$ mC/m^2,[33] but at a more than 2 times higher coercive field E_C. These differences might be a logical consequence of weaker dipole−dipole interaction in the present "diluted" OVDF-containing materials. The significant difference in remnant polarization between **Pc-OVDF** and **PBI-OVDF** can tentatively be explained by differences in the OVDF weight percentage per molecule and the amount of β-phase conformation. Therefore, we can tentatively conclude that the percentage of β-phase achieved, the crystallinity, and the dipole density affect the ferroelectric response of the materials. These influences were investigated in detail on PVDF,[34] for which also a reduction of the ferroelectric response as a result of adding a non-ferroelectric phase to the ferroelectric matrix has been observed.[35]

CONCLUSIONS

A synthetic method for the end-functionalization of OVDF has been developed, allowing the synthesis of three disc-shaped molecules substituted at the periphery with three, six, and eight oligomers of the well-known ferroelectric oligomer. The desired compounds were obtained in good yields via a radical reaction between terminal olefins and **I-OVDF**. The formation and purity of the final adducts have been confirmed by a combination of analytical techniques. The thermal behavior and the morphology of the materials have been also assessed. The conformation of the OVDF side chains of **BTA-OVDF**, **PBI-OVDF**, and **Pc-OVDF** within the materials has been analyzed by IR, observing, in all cases, the highest fraction of β-conformation after application of an electrical field at elevated temperatures, followed by slow cooling. For both **PBI-OVDF** and **Pc-OVDF**, ferroelectric hysteresis behavior was observed, with appreciable remnant polarization, especially for **Pc-OVDF**. Despite the formation of a dominant β-phase, **BTA-OVDF** did not show any ferroelectric behavior.

The reported examples demonstrate the possibility to prepare a new class of ferroelectric materials by attaching OVDF oligomers to different small semiconducting molecules. Combining two orthogonal properties, such as ferroelectricity and electrical conductivity, in a single compound can give rise to new and unprecedented functional materials. Studies using these materials in nonvolatile memory devices will be published elsewhere.[36]

ASSOCIATED CONTENT

Supporting Information

The Supporting Information is available free of charge on the ACS Publications website at DOI: 10.1021/jacs.6b01908.

Synthetic details and molecular characterization as well as device manufacturing and details of the ferroelectric measurements, including Figures S1−S36 (PDF)

AUTHOR INFORMATION

Corresponding Author

*e.w.meijer@tue.nl

Notes

The authors declare no competing financial interest.

ACKNOWLEDGMENTS

We thank Thomas Gonzalez (MRL-UCSB) for synthetic support and Stefan Meskers for stimulating discussions. The work was financed by the Dutch Polymer Institute (DPI No. 765), the Dutch Ministry of Education, Culture and Science (Gravity program 024.001.035), and the European Research Council (FP7/2007-2013, ERC Grant Agreement 246829).

REFERENCES

(1) Scott, J. F. *Science* **2007**, *315*, 954−959.

DOI: 10.1021/jacs.6b01908
J. Am. Chem. Soc. 2016, 138, 6217−6223

(2) Valasek, J. *Phys. Rev.* **1921**, *17*, 475−481.
(3) (a) Horiuchi, S.; Tokura, Y. *Nat. Mater.* **2008**, *7*, 357−366. (b) Horiuchi, S.; Tokunaga, Y.; Giovannetti, G.; Picozzi, S.; Itoh, H.; Shimano, R.; Kumai, R.; Tokura, Y. *Nature* **2010**, *463*, 789−792. (c) Tayi, A. S.; Shveyd, A. K.; Sue, A. C.-H.; Szarko, J. M.; Rolczynski, B. S.; Cao, D.; Kennedy, T. J.; Sarjeant, A. A.; Stern, C. L.; Paxton, W. F.; Wu, W.; Dey, S. K.; Fahrenbach, A. C.; Guest, J. R.; Mohseni, H.; Chen, L. X.; Wang, K. L.; Stoddart, J. F.; Stupp, S. I. *Nature* **2012**, *488*, 485−489. (d) Tayi, A. S.; Kaeser, A.; Matsumoto, M.; Aida, T.; Stupp, S. I. *Nat. Chem.* **2015**, *7*, 281−294.
(4) Lovinger, A. J. *Science* **1983**, *220*, 1115−1121.
(5) (a) Kawai, H. *Jpn. J. Appl. Phys.* **1969**, *8*, 975−976. (b) Calvert, P. *Nature* **1975**, *256*, 694.
(6) (a) Furukawa, T. *Phase Transitions* **1989**, *18*, 143−211. (b) Kepler, R. G.; Anderson, R. A. *Adv. Phys.* **1992**, *41*, 1−57. (c) Dubois, J.-C. *Adv. Mater.* **1996**, *8*, 542.
(7) El Mohajir, B.-E.; Heymans, N. *Polymer* **2001**, *42*, 5661−5667.
(8) (a) Wegener, M.; Gerhard-Multhaupt, R. *IEEE Trans.* **2003**, *50*, 921−931. (b) Arlt, K.; Wegener, M. *IEEE Trans. Dielectr. Electr. Insul.* **2010**, *17*, 1178−1184.
(9) (a) Umemoto, S.; Kikutani, T.; Okui, N. *Polym. J.* **1998**, *30*, 659−663. (b) Herman; Uno, T.; Kubono, A.; Umemoto, S.; Kikutani, T.; Okui, N. *Polymer* **1997**, *38*, 1677−1683.
(10) Noda, K.; Ishida, K.; Kubono, A.; Horiuchi, T.; Yamada, H.; Matsushige, K. *J. Appl. Phys.* **2003**, *93*, 2866−2870.
(11) (a) Noda, K.; Ishida, K.; Kubono, A.; Horiuchi, T.; Yamada, H.; Matsushige, K. *Jpn. J. Appl. Phys., Part 1* **2000**, *39*, 6358−6363. (b) Matsumoto, A.; Horie, S.; Yamada, H.; Matsushige, K.; Kuwajima, S.; Ishida, K. *Appl. Phys. Lett.* **2007**, *90*, 202906−202909.
(12) Kodama, H.; Takahashi, Y.; Furukawa, T. *Ferroelectrics* **1997**, *203*, 433−455.
(13) (a) Yanai, N.; Uemura, T.; Kosaka, W.; Matsuda, R.; Kodani, T.; Koh, M.; Kanemura, T.; Kitagawa, S. *Dalton Trans.* **2012**, *41*, 4195−4198. (b) Boschin, F.; Blanchemain, N.; Bria, M.; Delcourt-Debruyne, E.; Morcellet, M.; Hildebrand, H. F.; Martel, B. *J. Biomed. Mater. Res., Part A* **2006**, *79A*, 78−85.
(14) (a) Asadi, K.; de Leeuw, D. M.; de Boer, B.; Blom, P. W. M. *Nat. Mater.* **2008**, *7*, 547−550. (b) Naber, R. C. G.; Asadi, K.; Blom, P. W. M.; de Leeuw, D. M.; de Boer, B. *Adv. Mater.* **2010**, *22*, 933−945. (c) Fabiano, S.; Usta, H.; Forchheimer, R.; Crispin, X.; Facchetti, A.; Berggren, M. *Adv. Mater.* **2014**, *26*, 7438−7443.
(15) (a) Choi, T.; Lee, S.; Choi, Y. J.; Kiryukhin, V.; Cheong, S.-W. *Science* **2009**, *324*, 63−66. (b) Yuan, Y.; Reece, T. J.; Sharma, P.; Poddar, S.; Ducharme, S.; Gruverman, A.; Yang, Y.; Huang, J. *Nat. Mater.* **2011**, *10*, 296−302. (c) Yuan, Y.; Reece, T. J.; Sharma, P.; Poddar, S.; Ducharme, S.; Gruverman, A.; Yang, Y.; Huang, J. *Nat. Mater.* **2011**, *10*, 296−302. (d) Yuan, Y.; Xiao, Z.; Yang, B.; Huang, J. *J. Mater. Chem. A* **2014**, *2*, 6027−6041.
(16) (a) Feng, X.; Marcon, V.; Pisula, W.; Hansen, M. R.; Kirkpatrick, J.; Grozema, F.; Andrienko, D.; Kremer, K.; Müllen, K. *Nat. Mater.* **2009**, *8*, 421−426. (b) Pisula, W.; Feng, X.; Müllen, K. *Adv. Mater.* **2010**, *22*, 3634−3649.
(17) (a) Sugita, A.; Suzuki, K.; Tasaka, S. *Chem. Phys. Lett.* **2004**, *396*, 131−135. (b) Fitié, C. F. C.; Roelofs, W. S. C.; Kemerink, M.; Sijbesma, R. P. *J. Am. Chem. Soc.* **2010**, *132*, 6892−6893. (c) Fitié, C. F. C.; Roelofs, W. S. C.; Magusin, P. C. M. M.; Wübbenhorst, M.; Kemerink, M.; Sijbesma, R. P. *J. Phys. Chem. B* **2012**, *116*, 3928−3937.
(18) (a) Gsänger, M.; Oh, J. H.; Könemann, M.; Höffken, H. W.; Krause, A.-M.; Bao, Z.; Würthner, F. *Angew. Chem.* **2010**, *122*, 752−755. (b) Chen, Z.; Baumeister, U.; Tschierske, C.; Würthner, F. *Chem. - Eur. J.* **2007**, *13*, 450−465. (c) Claessens, C.; Blau, W.; Cook, M.; Hanack, M.; Nolte, R. M.; Torres, T.; Wöhrle, D. In *Molecular Materials and Functional Polymers SE-1*; Blau, W., Lianos, P., Schubert, U., Eds.; Springer: Vienna, 2001; pp 3−11.
(19) (a) Elemans, J. A. A. W.; van Hameren, R.; Nolte, R. J. M.; Rowan, A. E. *Adv. Mater.* **2006**, *18*, 1251−1266. Semiconducting properties of perylenes bisimides: (b) Zhang, M.-X.; Zhao, G.-J. *ChemSusChem* **2012**, *5*, 879−887. (c) Jones, B. A.; Ahrens, M. J.; Yoon, M.-H.; Facchetti, A.; Marks, T. J.; Wasielewski, M. R. *Angew. Chem., Int. Ed.* **2004**, *43*, 6363−6366. (d) Malenfant, P. R. L.; Dimitrakopoulos, C. D.; Gelorme, J. D.; Kosbar, L. L.; Graham, T. O.; Curioni, A.; Andreoni, W. *Appl. Phys. Lett.* **2002**, *80*, 2517−2519. Semiconducting properties of phthalocyanines: (e) Eley, D. D. *Nature* **1948**, *162*, 819. (f) Claessens, C. G.; Hahn, U.; Torres, T. *Chem. Rec.* **2008**, *8*, 75−97.
(20) Vukićević, R.; Hierzenberger, P.; Hild, S.; Beuermann, S. *J. Polym. Sci., Part A: Polym. Chem.* **2010**, *48*, 4847−4854.
(21) Yanai, N.; Uemura, T.; Uchida, N.; Bracco, S.; Comotti, A.; Sozzani, P.; Kodani, T.; Koh, M.; Kanemura, T.; Kitagawa, S. *J. Mater. Chem.* **2011**, *21*, 8021−8025.
(22) Qi, Q.; Shen, Q.; Lu, L. *J. Am. Chem. Soc.* **2012**, *134*, 6548−6551.
(23) (a) Boyer, C.; Valade, D.; Sauguet, L.; Ameduri, B.; Boutevin, B. *Macromolecules* **2005**, *38*, 10353−10362. (b) Araki, T.; Kodani, T. Method of forming thin film. WO Patent 2004085498, October 7, 2004. (c) Voet, V. S. D.; ten Brinke, G.; Loos, K. *J. Polym. Sci., Part A: Polym. Chem.* **2014**, *52*, 2861−2877.
(24) (a) Lopes, A. C.; Costa, C. M.; Tavares, C. J.; Neves, I. C.; Lanceros-Mendez, S. *J. Phys. Chem. C* **2011**, *115*, 18076−18082. (b) Li, M.; Wondergem, H. J.; Spijkman, M.-J.; Asadi, K.; Katsouras, I.; Blom, P. W. M.; de Leeuw, D. M. *Nat. Mater.* **2013**, *12*, 433−438.
(25) Chellappan, K. V.; Kandappa, S. K.; Rajaram, S.; Narayan, K. S. *J. Phys. Chem. Lett.* **2015**, *6*, 224−229.
(26) Mangialardo, S.; Larciprete, M. C.; Belardini, a.; Sibilia, C.; Bertolotti, M. *Laser Phys.* **2008**, *18*, 1371−1377.
(27) Nalwa, H. S., Ed. *Ferroelectric Polymers: Chemistry, Physics, and Applications*; Dekker: New York, 1995.
(28) (a) Fukunaga, M.; Noda, Y. *J. Phys. Soc. Jpn.* **2008**, *77*, 064706. (b) Khikhlovskyi, V.; Gorbunov, A. V.; van Breemen, A. J. J. M.; Janssen, R. A. J.; Gelinck, G. H.; Kemerink, M. *Org. Electron.* **2013**, *14*, 3399−3405.
(29) Lenz, T.; Zhao, D.; Richardson, G.; Katsouras, I.; Asadi, K.; Glaßer, G.; Zimmermann, S. T.; Stingelin, N.; Roelofs, W. S. C.; Kemerink, M.; Blom, P. W. M.; de Leeuw, D. M. *Phys. Status Solidi A* **2015**, *212*, 2124−2132.
(30) For both materials, no ferroelectric switching has been observed for temperatures below those mentioned in the text, nor above the temperature of the isotropic phase transition.
(31) (a) Dias, C. J.; Inácio, P.; Marat-Mendes, J. N.; Das-Gupta, D. K. *Ferroelectrics* **1997**, *198*, 121−130. (b) Wenger, M. P.; Almeida, P. L.; Das-Gupta, D. K.; Blanas, P.; Shuford, R. J. *Polym. Eng. Sci.* **1999**, *39*, 483−492. (c) Xin, C.; Shifeng, H.; Jun, C.; Zongjin, L. J. *J. Appl. Phys.* **2007**, *101*, 094110−094110.
(32) Bharti, V.; Kaura, T.; Nath, R. *IEEE Trans. Dielectr. Electr. Insul.* **1997**, *4*, 738−741.
(33) Chen, S.; Yao, K.; Hock Tay, F. E. *Polym. Int.* **2012**, *61*, 169−173.
(34) Gomes, J.; Nunes, J. S.; Sencadas, V.; Lanceros-Mendez, S. *Smart Mater. Struct.* **2010**, *19*, 065010.
(35) (a) Khan, M. A.; Bhansali, U. S.; Almadhoun, M. N.; Odeh, I. N.; Cha, D.; Alshareef, H. N. *Adv. Funct. Mater.* **2014**, *24*, 1372−1381. (b) Soulestin, T.; Ladmiral, V.; Lannuzel, T.; Dos Santos, F. D.; Ameduri, B. *Macromolecules* **2015**, *48*, 7861−7871.
(36) Gorbunov, A. V.; Garcia Iglesias, M.; Guilleme, J.; Roelofs, W. S. C.; Torres, T.; González-Rodríguez, D.; Meijer, E. W.; Kemerink, M. Manuscript submitted.

DOI: 10.1021/jacs.6b01908
J. Am. Chem. Soc. 2016, 138, 6217−6223